NASA Technical Memorandum 4163

Optimum Element Density Studies for Finite-Element Thermal Analysis of Hypersonic Aircraft Structures

William L. Ko, Timothy Olona,
and Kyle M. Muramoto

JANUARY 1990

NASA

NASA Technical Memorandum 4163

Optimum Element Density Studies for Finite-Element Thermal Analysis of Hypersonic Aircraft Structures

William L. Ko, Timothy Olona,
and Kyle M. Muramoto
Ames Research Center
Dryden Flight Research Facility
Edwards, California

NASA
National Aeronautics and
Space Administration
Office of Management
Scientific and Technical
Information Division

1990

CONTENTS

ABSTRACT

Different finite-element models previously set up for thermal analysis of the space shuttle orbiter structure were discussed and their shortcomings were identified. Element density criteria were established for the finite-element thermal modelings of space shuttle orbiter-type large, hypersonic aircraft structures. These criteria were based on rigorous studies on solution accuracies using different finite-element models having different element densities set up for one cell of the orbiter wing. Also, a method for optimization of the transient thermal analysis computer central processing unit (CPU) time was discussed. Based on the newly established element density criteria, the orbiter wing midspan segment was modeled for the examination of thermal analysis solution accuracies and the extent of computation CPU time requirements. The results showed that the distributions of the structural temperatures and the thermal stresses obtained from this wing segment model were satisfactory and the computation CPU time was at the acceptable level. The studies offered the hope that modeling the large, hypersonic aircraft structures using high-density elements for transient thermal analysis was possible if a CPU optimization technique was used.

INTRODUCTION

During the early stage of space shuttle development, the heat transfer analysis of the complex orbiter structure was carried out by using the so-called "plug" method. Only selected small, local regions of the orbiter were modeled with three-dimensional finite-difference (or lumped parameters) plug thermal models (fig. 1). Structural temperatures calculated from the plug models were then interpolated to obtain structural temperatures in the unmodeled regions. Approximately 90 percent of the temperature inputs used in the early days of orbiter thermal stress analysis was obtained by this type of interpolation. The procedure was tedious, laborious, and expensive. For structures with steep temperature gradients near the heat sinks (for example, the orbiter wing spar and rib caps), the structural temperature distribution obtained from the interpolation method could be erroneous and could cause inaccurate thermal stress predictions.

After the development of finite-element heat transfer analysis computer codes such as the structural performance and resizing (SPAR) finite-element thermal analysis computer program (ref. 1), it became possible to model larger regions of the orbiter structure including the whole wing. The use of the finite-element method instead of the conventional lumped-parameter (or finite-difference) method enables the use of the same thermal model as a structural model for thermal stress calculations by simply removing elements set up for the thermal protection system (TPS) (not a major mechanical load-carrying structural component). In the past several years, Ko and others (refs. 2 to 9) conducted extensive heat transfer and thermal stress analyses of the space shuttle orbiter using a series of finite-element models set up for three wing segments, one fuselage cross section, and the whole wing. These thermal models were used to calculate orbiter structural temperatures which were correlated with the actual flight-measured data during the initial orbiter tests of the space shuttle Columbia (refs. 2 to 8). The earlier thermal models set up for the orbiter structure were by no means perfect and had shortcomings in the light of element density, element size distributions, and extent of the region modeled.

In the finite-element heat transfer and thermal stress analysis of small structural components, the element density may be freely increased at will to obtain highly accurate solutions without the worry that the limit of the computer memory core space might be reached or exceeded. However, in the finite-element thermal modeling of large, hypersonic aircraft structures (such as the space shuttle and space plane), the use of high-density finite elements could increase the number of radiation view factors tremendously, and could require prohibitive computer time and/or computer core space requirements in the transient heat transfer analysis using these radiation view factors. In the wing box-type structures, each time the number of radiation elements is doubled, the number of radiation view factors would be nearly quadrupled. Thus, in the finite-element heat transfer analysis of large aerospace structures, the highest desirable element density is governed by the time requirement and/or by the memory capacity of the computer used. The corresponding structural model for thermal stress analysis using the same element density as

the thermal model has far less nodal points because the non-load-carrying heat shields are removed. It is, therefore, not the model to be used to set up the criteria for maximum allowable element density. Preliminary studies in this area were carried out by Ko and others (refs. 10 to 12) to investigate solution accuracies obtained from different finite-element models having different element densities set up for one wing cell of the orbiter. These studies formed the foundation of the state of the art in finite-element modelings of large, hypersonic aircraft structures.

In this report, several past finite-element models set up for the orbiter structure are reviewed and their shortcomings are identified. The criteria for the element density and element size distribution required for finite-element modeling of larger orbiter wing regions are discussed in detail. Finally, the report shows how to optimize the SPAR transient heat transfer analysis computation CPU time when the high-density elements are used.

NOMENCLATURE

C	capacitance matrix
C21	two-node forced convection element
C41	four-node forced convection element
CPU	central processing unit
CQUAD2	quadrilateral membrane and bending element
CROD	two-node tension–compression–torsion element
E23	bar elements
E25	zero-length element for elastically connected, geometrically coincident joints
E31	triangular membrane element
E41	quadrilateral membrane element
E44	quadrilateral shear panel element
F_{ij}	radiation view factor from element i to element j
FRSI	flexible felt reusable surface insulation
H	convection load vector
HRSI	high temperature reusable surface insulation
i	integer, 1, 2, 3, ...
JLOCS	joint locations
j	integer, 1, 2, 3, ...
K	system matrix = $K_k + K_r + K_h$
K_h	convection matrix
K_k	conduction matrix
K_r	radiation matrix
K21	two-node line conduction element
K31	three-node area conduction element
K41	four-node area conduction element
K61	six-node volume conduction element
K81	eight-node volume conduction element

KTIME	control command in SPAR computer program to specify the time interval at which the system matrix K is to be factored
LRSI	low temperature reusable surface insulation
NASTRAN	NASA structural analysis
Q	source load vector
R	radiation load vector
R21	two-node area radiation element
R31	three-node area radiation element
R41	four-node area radiation element
RCONV	control command in SPAR computer program to set the convergence criterion for the radiation load vector computations
RNITER	control command in SPAR computer program to set the maximum number of iterations permitted during the computations of radiation load vectors
RTIME	control command in SPAR computer program to specify the time increments at which the radiation load vectors are to be computed
SIP	strain isolation pad
SPAR	structural performance and resizing
STS-5	space transportation system, flight 5
T	absolute temperature
T_2	final time of SPAR transient thermal analysis
TPS	thermal protection system
Y_o	station in y-axis
$[\dot{}]$	time derivative
σ_x	chordwise stress
σ_y	spanwise stress
τ_{xy}	shear stress

REVIEW OF PAST MODELS

Wing and Fuselage Cross Sections

Figures 2 and 3 show two typical past thermal models (WS240, FS877) set up for the orbiter wing midspan and midfuselage cross sections (ref. 5). The corresponding structural models were obtained by removing the TPS elements. In both figures, the sizes of the thermal and the corresponding structural models are compared. Notice that the structural models are always simpler (less nodal points). These thermal models were extensively used to calculate orbiter structural temperatures which were correlated with the actual flight data obtained from initial orbital tests of the space shuttle Columbia (refs. 2 to 8). The WS240 model (fig. 2) has a reasonable number of elements to give satisfactory structural temperature distributions in the chordwise direction, but not in the spanwise direction. Also, the FS877 model (fig. 3), which is two-dimensional, can give good structural temperature distribution in the fuselage circumferential direction, but not in the fuselage axial direction.

Both of these thermal models, when converted to structural models by removing TPS elements, are not capable of yielding accurate thermal stress predictions because of the following reasons. It is well known that the magnitudes of the computed thermal stresses are sensitive to the modeling parameters (such as element density, element size distributions, and extent of the region modeled) (refs. 11 and 12). For the case of biaxial stress fields which occur in orbiter-type structures (especially wing and fuselage skins), the manner in which the boundary conditions are applied can greatly affect the magnitudes of calculated thermal stresses in the proximity of the tracted boundaries or free edges. Because the thermal stresses attenuate to zero at free edges, the structural models must have dimensions sufficiently large enough to be beyond the influence of the edge effects. Both models mentioned earlier lack the capacity to fulfill those structural modeling requirements.

Whole Wing

In order to eliminate the modeling shortcomings that occurred in the WS240 models (thermal and structural), the whole wing of the orbiter was modeled (refs. 8 and 9). Figure 4 shows the past thermal model, WING, set up for the orbiter whole wing. In the figure the sizes of both the thermal model and the structural model (TPS landing gear and wheel well door elements removed) are compared. In this case the number of nodes for the structural model is approximately 10 percent of that of the thermal model.

Because of the fear of encountering and dealing with a tremendous number of radiation view factors, the element sizes used in the WING model were relatively coarse. The WING thermal model required 48,034 radiation view factor computations and can only give "roof"-shaped structural temperature distributions. Therefore, the thermal stresses calculated based on this type of temperature distribution may not give accurate predictions. Thus, finer elements are required for the whole wing model, for which the optimum manageable element density has to be determined first.

ELEMENT DENSITY

Because of the need of finding the optimum element density and element size distribution for modeling orbiter whole wing-type structures, Ko and others (refs. 11 and 12) set up five different finite-element models (A, B, C, D, and E) with different element densities for one orbiter wing cell (located at midspan bay 3 (fig. 5)), and examined the effect of element density on the finite-element solution accuracies. These studies laid the foundation, or state of the art, for choosing optimum element density in finite-element modeling of whole orbiter wing-type structures.

Figure 6 shows the wing's lower skin temperature distributions predicted from the five thermal models. Except for model A, which had the same skin element density as that of the WING model (fig. 4), models B, C, D, and E gave very close values of the structural temperatures at the center region of the wing's lower skin.

Figure 7 shows how the number of radiation view factors F_{ij} increases as the number of radiation elements R41 (or element density) increases. For this particular type of wing cell structure, doubling the number of radiation elements R41 would cause the number of radiation view factors F_{ij} to nearly quadruple.

Model E gives smooth structural temperature distribution (fig. 6), and its element density level can be considered an attractive element density to use in modeling the whole orbiter wing-type structures. However, the SPAR transient heat transfer analysis using model E required extremely long computer CPU time because of the computations of the time-dependent radiation exchange vector using the 93,868 radiation view factors F_{ij}. Thus, the use of model E element density level in modeling the whole orbiter wing-type structures could be beyond the current computer capabilities (memory core space and computation speed).

The structural temperature distribution given by model E has a flat region near the wing skin central region in the chordwise direction. In this region, slightly coarser elements, as in the element density level of model D, could be used to reduce CPU time without sacrificing the solution accuracy. As shown in the Central Processing Unit

Time Optimization section of this report, the SPAR CPU time for model D is 21 to 27 percent of that for model E. The logical criteria for setting the element density and size distribution for modeling large, complex aerospace structures could be somewhere between the element density levels of models D and E (for example, eight elements in chordwise direction and six elements in spanwise direction, with finer elements located near the heat sinks).

CENTRAL PROCESSING UNIT TIME OPTIMIZATION

In the finite-element transient heat transfer analysis using the SPAR program, the governing matrix equation used is of the form (ref. 1)

$$(K_k + K_r + K_h)T + C\dot{T} = Q + R + H \tag{1}$$

where

K_k	is the conduction matrix,
K_r	the radiation matrix,
K_h	the convection matrix,
T	the absolute temperature,
C	the capacitance matrix,
Q	the source load vector,
R	the radiation load vector,
H	the convection load vector, and
$[\dot{}]$	denotes time derivative.

In the computations using equation (1), there are several key control parameters which could be adjusted to reduce the SPAR CPU time. However, at the same time the solution accuracy may be affected by adjusting those control parameters. Therefore, it is vital to find out the optimum values of those control parameters which will drastically reduce the SPAR CPU time and yet will hardly affect the solution accuracy. Those control parameters are:

KTIME = control command to specify the time interval at which the system matrix $K(= K_k + K_r + K_h)$ is to be factored (see eq. (1)).

RTIME = control command to specify the time increments at which the radiation load vectors (R) are to be computed (see eq. (1)).

RCONV = control command to set the convergence criterion for the radiation load vector computations.

RNITER = control command to set the maximum number of iterations permitted during the computation of radiation load vectors (R).

Figure 8 shows the SPAR transient thermal analysis (up to 3000 sec from reentry) computation CPU time (using the ELXSI 6400 computer) plotted as a function of the number of joint locations of thermal models for two sets of KTIME/RTIME values. By increasing both the values of KTIME and RTIME from 2 sec to 25 sec, the SPAR CPU time could be drastically reduced, and the solutions remain practically unchanged. The peak skin temperatures and actual SPAR CPU time associated with the different thermal models are tabulated in table 1. Notice that the use of model E, which required a SPAR CPU time several times longer than that for model D, did not show any advantage in solution accuracy.

Table 1. SPAR computation CPU time and peak skin temperatures associated with different wing cell thermal models.

Model	KTIME = RTIME, sec			
	SPAR CPU time, min		Peak skin temperature, °F	
	2	25	2	25
A	19.38	5.48	101.11	101.07
B	102.13	23.18	117.25	117.27
C	177.87	35.88	117.17	117.20
D	301.02	56.45	117.26	117.30
E	1428.08	204.28	117.36	117.42

For conducting a more thorough study of the effects of KTIME, RTIME, and other SPAR control parameters previously mentioned, and for finding the optimum values of these parameters, the thermal model D (fig. 5) was used because it required much less SPAR CPU time than model E.

Table 2. SPAR computation CPU times and peak skin temperatures based on thermal model D.

KTIME, sec	RTIME, sec	RCONV	RNITER	SPAR CPU time, min	Peak skin temperature, °F
2	2	0.0001	12	301.02	117.26
10				231.08	117.36
25				219.95	117.44
50				218.15	117.36
100				216.53	116.55
25[a]	10			79.90	117.39
	25[a]			56.45	117.30
			10	56.63	117.30
			8	56.90	117.30
			5[b]	---	---[c]
		0.0005	12	53.98	116.78
		0.001[b]		52.77	116.24
	50	0.0001		50.10	117.15
	100			47.02	116.87
50	50			45.48	117.07

[a]Optimum KTIME and RTIME.
[b]Default value.
[c]Radiation exchange vectors did not converge.

Table 2 summarizes the results of this investigation. Figure 9 shows the data of table 2 plotted in the KTIME/RTIME space. Notice that by increasing KTIME from 2 sec to 25 scc (holding RTIME = 2 sec), the SPAR CPU time could be reduced from 301.02 min (point A) down to 219.95 min (point B). This is an approximately 27-percent reduction in SPAR CPU time. Further increase in the value of KTIME offered very little gain in saving SPAR CPU time. Next, by increasing RTIME from 2 sec to 25 sec (keeping KTIME = 25 sec), the SPAR CPU time could be further reduced from 219.95 min (point B) down to 56.45 min (point C). This gives another 54-percent reduction (based on point A) in the SPAR CPU time without affecting the solution accuracy. Further increase in the value of

RTIME beyond point C did not save much SPAR CPU time. At point C the SPAR CPU time is only 19 percent of that at point A, and the solution error is only 0.04 °F (compared to that at point A). Additional increase in both values of KTIME and RTIME to 50 sec (point D) had very little improvement in CPU time, and the solution error started to show up (0.19 °F error). Thus, point C could be chosen as the optimum point for selecting the values of KTIME and RTIME. The reductions of the values of RCONV and RNITER from 0.0001 and 12, respectively, had little effect on the improvement of the SPAR CPU time (table 2).

MIDSPAN MODEL

Element Density

Based on the knowledge gained from the studies of element density requirements and the SPAR CPU time optimization described earlier, the element density criteria is established for the finite-element modelings of the orbiter wing-type structures. Before modeling the orbiter whole wing with high-density elements, it is wise to first model one segment of the orbiter wing with high-density elements and explore the CPU time requirements in the SPAR transient thermal analysis. The CPU time found for the wing segment model may then be extrapolated to estimate the CPU time requirement for the whole wing model having the same element density as the wing segment model. The said wing segment has four bays and is located at the midspan bounded by two adjacent wing ribs located at Y_o-226 and Y_o-254, respectively.

The thermal model MIDSPAN for this wing segment is shown in figure 10. In the light of structural temperature distributions obtained from models D and E (fig. 6), the lower and upper skins of each bay of the wing segment were modeled with eight and six different-sized elements, respectively, in the chordwise and spanwise directions with finer elements used near the heat sinks (spar and rib caps). The MIDSPAN SPAR thermal model has 4064 joint locations, 1149 radiation elements R41, and 137,328 radiation view factors F_{ij}. The corresponding NASTRAN (ref. 13) structural model has 722 grid points (18 percent of the thermal model). The sizes of the MIDSPAN thermal and structural models are compared in table 3.

Table 3. Summary of thermal and structural models for an orbiter wing midspan segment.

Item	Model	
	Thermal	Structural
Number of nodes	4,046	722
Number of elements	363 K21	674 CQUAD2
	1,634 K41	303 CROD
	6 K61	
	2,730 K81	
	1,149 R41	
	764 C41	
Number of F_{ij}	137,328	---
Total CPU time, min[a]	464	13
F_{ij} computation CPU time, min	38	---

[a]ELXSI 6400 computer
KTIME = RTIME = 25 sec
RCONV = 0.0001, RNITER = 12
T_2 = 3000 sec

Central Processing Unit Time

By using the previously established optimum values of KTIME = RTIME = 25 sec, transient heat transfer analysis was performed on the MIDSPAN thermal model. This thermal model required 464 min computation CPU time (table 3) for the thermal analysis duration of 3000 sec. The corresponding structural model took 13 min computation CPU time. It took only 38 min to compute the vast number (137,328) of radiation view factors. It must be emphasized that once the radiation view factors are computed, they are stored in the computer file, and no more computations are required in subsequent computer runs of the same thermal model. Therefore, in the transient thermal analysis most of the computation CPU time is used in computing time-dependent structural temperatures, not in computing radiation view factors, even though their number is enormous. This finding eliminated the fear of encountering a huge number of view factors in the thermal modelings of large, complex aerospace structures using finer elements.

Structural Temperatures

The calculations of the structural temperatures in the MIDSPAN thermal model were based on the STS-5 surface heating rates shown in figure 11. The distributions of skin temperatures in time sequence are shown in figure 12. The most severe (highest values and gradients) temperature distributions occurred at 1700 sec from reentry, and gradually the severity tapered off as the time increased. Judging from the temperature distribution surfaces for each bay, the use of an 8 by 6 system of element density gave acceptable smoothness of the skin temperature distributions. Therefore, an 8 by 6 system of element density could be considered as the element density criteria for modeling such types of aerospace structures.

Thermal Stresses

Based on the structural temperature distributions at 1700 sec, the thermal stresses σ_x, σ_y, and τ_{xy} in the wing skins were calculated and are shown in figures 13 to 15, respectively. Again the distributions of all three stresses exhibited acceptable smoothness, emphasizing that 8 by 6 system element density criteria were satisfactory. Notice that σ_x, whose direction is transverse to the hat stringers of the wing skins, has a higher magnitude than that of σ_y, and is therefore more critical.

Thermal Deformations

Figure 16 shows the undeformed and deformed shapes of the MIDSPAN structural model. The lower and upper skins of each bay bulged outwardly, with the maximum displacement of 0.08552 in. occurring near the midregion bay 1's upper skin. This amount of deformation is way below the thickness (0.16 in.) of the SIP. A small region in bay 1's upper skin, near the spar cap separating bays 1 and 2, dented slightly inward. By observing figure 16, the MIDSPAN structural model gave an acceptable detailed deformation field.

CONCLUSIONS

The element density level required in the finite-element thermal analysis of orbiter wing-type structures was investigated, and the optimization of transient thermal analysis computation central processing unit (CPU) time was discussed. The newly established element density criteria for each wing cell were eight elements in the chordwise direction and six elements in the spanwise direction. The resulting distributions of structural temperatures, thermal stresses, and thermal displacements were found to be satisfactory by using this level of element density in the thermal modeling of an orbiter wing segment.

The computation CPU time required for calculating the large number of radiation view factors comprised a small fraction of the total CPU time required for the computation of time-dependent structural temperatures. The study of the wing segment model, using the computer CPU time optimization technique, shows that the estimated computation CPU time required for the thermal analysis of the whole orbiter wing-type structures (with an 8 by 6 element density system) may be within the acceptable range.

Ames Research Center
Dryden Flight Research Facility
National Aeronautics and Space Administration
Edwards, California, August 22, 1988

REFERENCES

1. Marlowe, M.B.; Moore, R.A.; and Whetstone, W.D. : *SPAR Thermal Analysis Processors Reference Manual.* NASA CR-159162, vol. 1, 1979.

2. Ko, William L.; Quinn, Robert D.; Gong, Leslie; Schuster, Lawrence S.; and Gonzales, David: "Preflight Reentry Heat Transfer Analysis of Space Shuttle." AIAA-81-2382, AIAA/SETP/SFTE/SAE First Flight Testing Conference, Las Vegas, Nevada, Nov. 11–13, 1981.

3. Ko, William L.; Quinn, Robert D.; Gong, Leslie; Schuster, Lawrence S.; and Gonzales, David: "Reentry Heat Transfer Analysis of the Space Shuttle Orbiter." *Computational Aspects of Heat Transfer in Structures.* NASA CP-2216, 1982, pp. 295–325.

4. Gong, Leslie; Quinn, Robert D.; and Ko, William L.: "Reentry Heating Analysis of Space Shuttle With Comparison of Flight Data." *Computational Aspects of Heat Transfer in Structures.* NASA CP-2216, 1982, pp. 271–294.

5. Ko, William L.; Quinn, Robert D.; and Gong, Leslie: *Finite-Element Reentry Heat-Transfer Analysis of Space Shuttle Orbiter.* NASA TP-2657, 1986.

6. Gong, Leslie; Ko, William L.; and Quinn, Robert D.: *Comparison of Flight-Measured and Calculated Temperatures on the Space Shuttle Orbiter.* NASA TM-88278, 1987.

7. Ko, William L.; Quinn, Robert D.; and Gong, Leslie: *Effect of Internal Convection and Internal Radiation on the Structural Temperatures of Space Shuttle Orbiter.* NASA TM-100414, 1988.

8. Gong, Leslie; Ko, William L.; and Quinn, Robert D.: "Thermal Response of Space Shuttle Wing During Reentry Heating." AIAA-84-1761, AIAA 19th Thermophysics Conference, Snowmass, Colorado, June 25–28, 1984. Also published as NASA TM-85907, 1984.

9. Ko, William L.; and Fields, Roger A.: *Thermal Stress Analysis of Space Shuttle Orbiter Subjected to Reentry Aerodynamic Heating.* NASA TM-88286, 1987.

10. Polesky, Sandra P.; Robinson, James C.; and Ko, William L.: "Thermal Finite Element Analysis for Hypersonic Aircraft Structures." Presented at Third National Aero-Space Plane Technology Symposium, Moffett Field, California, June 2–4, 1987.

11. Ko, William L.; and Olona, Timothy: "Effect of Element Size on the Solution Accuracies of Finite-Element Heat Transfer and Thermal Stress Analyses of Space Shuttle Orbiter." *Proceedings of the Fifth International Conference on Numerical Methods for Thermal Problems.* Montreal, Quebec, Canada, June 29–July 3, 1987, vol. 5, pt. 2, July 1987, pp. 1114–1130. Also published as NASA TM-88292, 1987.

12. Ko, William L.: "Solution Accuracies of Finite Element Reentry Heat Transfer and Thermal Stress Analyses of Space Shuttle Orbiter." Special issue on "Numerical Methods in Thermal Problems," *International Journal for Numerical Methods in Engineering*, Sept. 1988.

13. *The NASTRAN User's Manual (Level 17.5).* NASA SP-222(05), 1978.

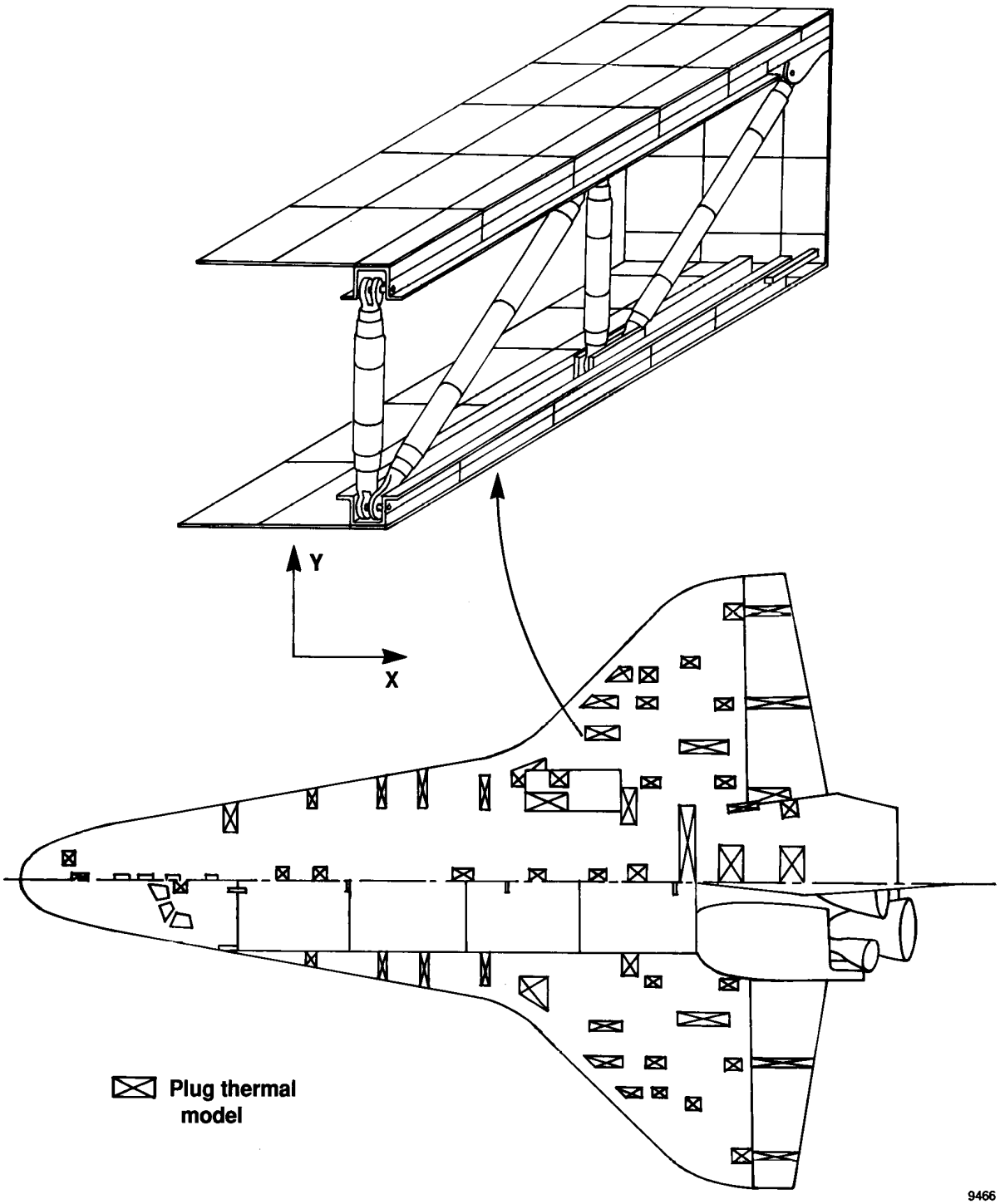

Figure 1. Locations of local three-dimensional plug thermal models for space shuttle orbiter.

Thermal model		Structural model	
Feature	Number	Feature	Number
JLOC	920	GRID point	204
K21 element	139	CROD element	139
K41 element	294	CQUAD2 element	121
K61 element	1		
K81 element	341		
R41 element	137		
C41 element	88		
F_{ij}	1680		

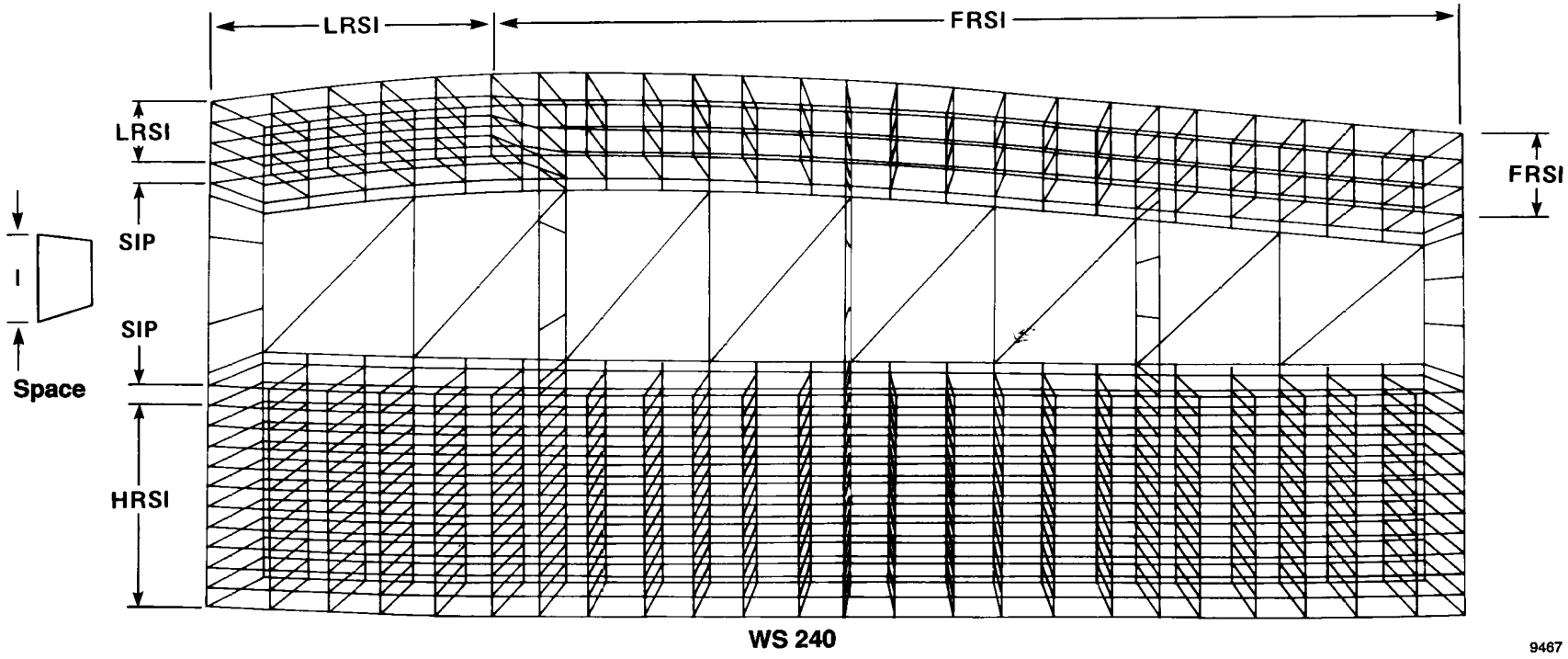

Figure 2. SPAR thermal model WS240 setup for orbiter wing midspan cross section. TPS elements removed to convert to structural model (ref. 5).

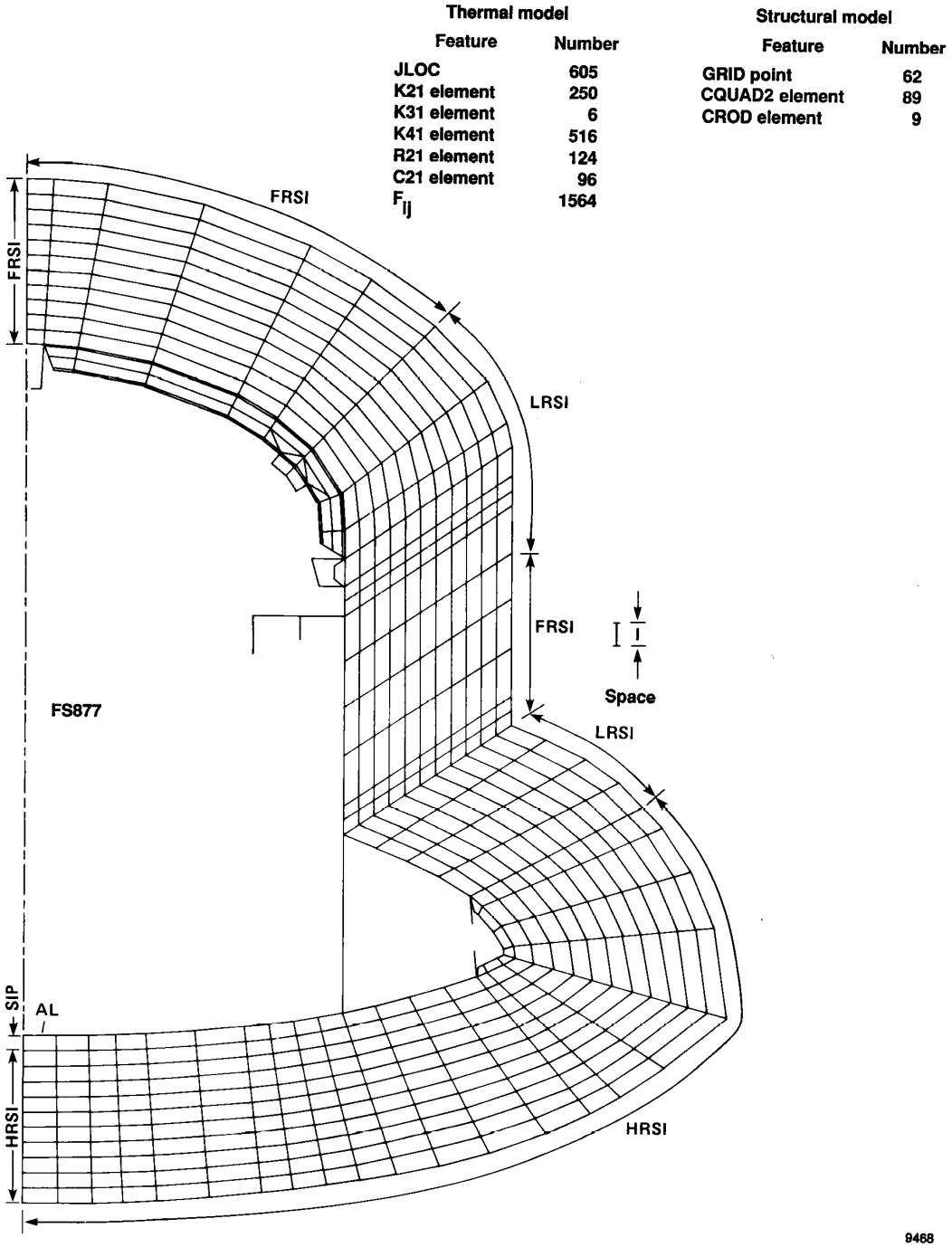

Figure 3. SPAR thermal model FS877 setup for orbiter midfuselage cross section. TPS and cargo bay door elements removed to convert to structural model (ref. 5).

Thermal model		Structural model	
Feature	Number	Feature	Number
JLOC	2289	JLOC	232
K21 element	1696	E23 element	498
K31 element	84	E25 element	10
K41 element	485	E31 element	19
R31 element	84	E41 element	181
R41 element	568	E44 element	67
F_{ij}	48,034		

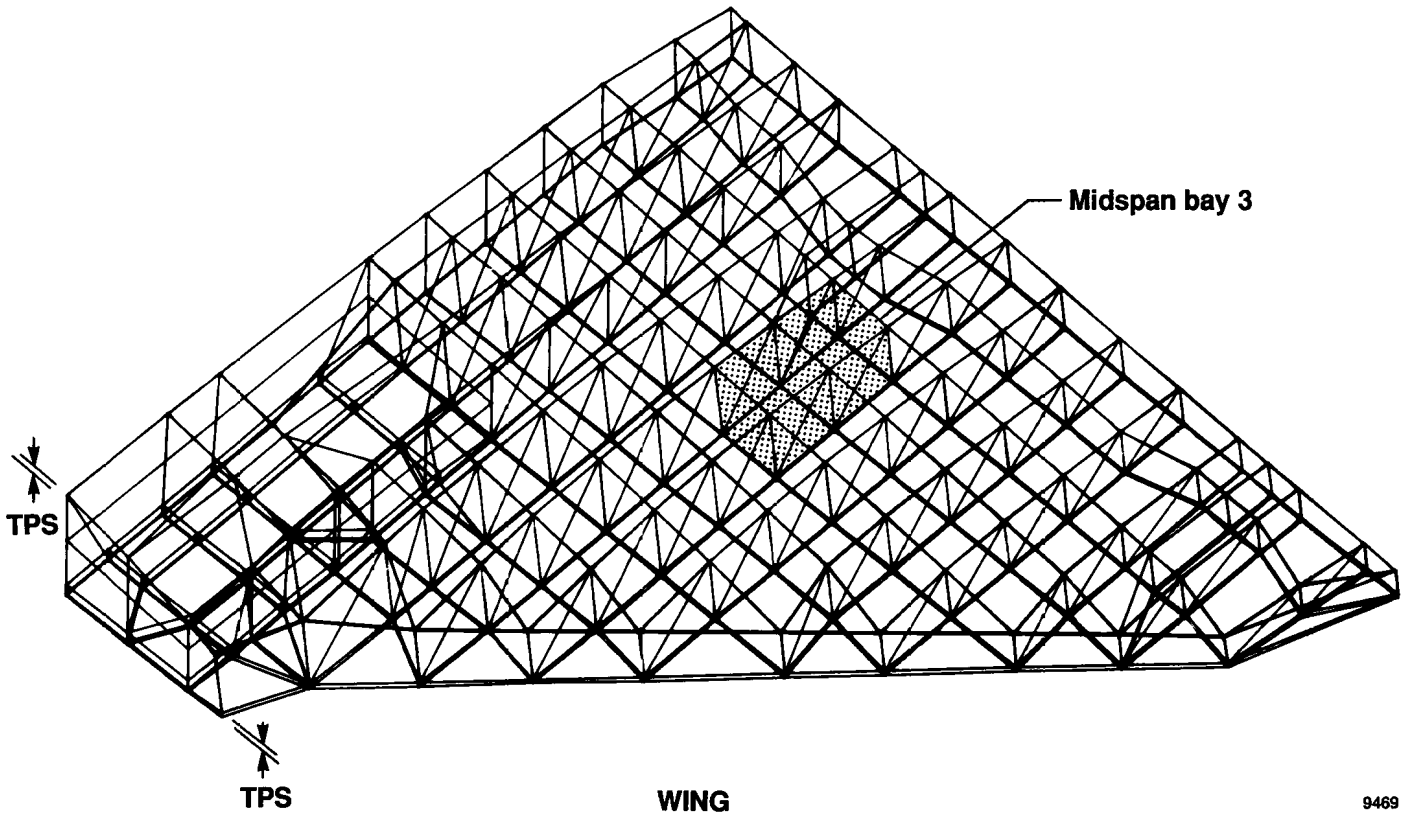

Figure 4. SPAR thermal model WING setup for orbiter wing. TPS, wheel well door, and landing gear removed to convert to structural model (refs. 8 and 9).

SPAR thermal model	JLOC	Element					F_{ij}
		K21	K41	K81	R41	C41	
A	112	34	28	28	15	10	78
B	436	54	168	224	89	56	2816
C	636	82	232	336	137	88	6894
D	972	98	360	560	201	120	13500
E	2076	146	848	1344	513	320	93869

NASTRAN structural model	Grid	CQUAD2	CROD
A	24	18	54
B	82	72	54
C	140	112	74
D	196	160	90
E	429	368	132

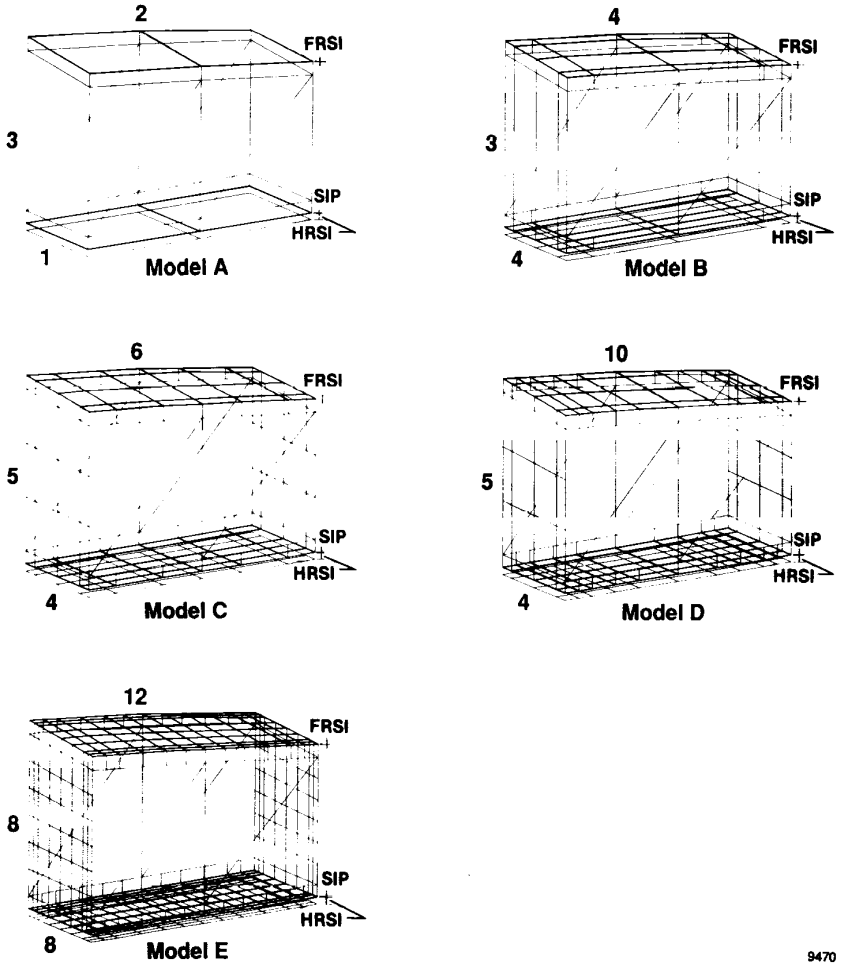

Figure 5. SPAR thermal models A, B, C, D, E setups for orbiter wing midspan bay 3. The K81 elements for TPS and SIP not shown; TPS and SIP removed to convert to structural models.

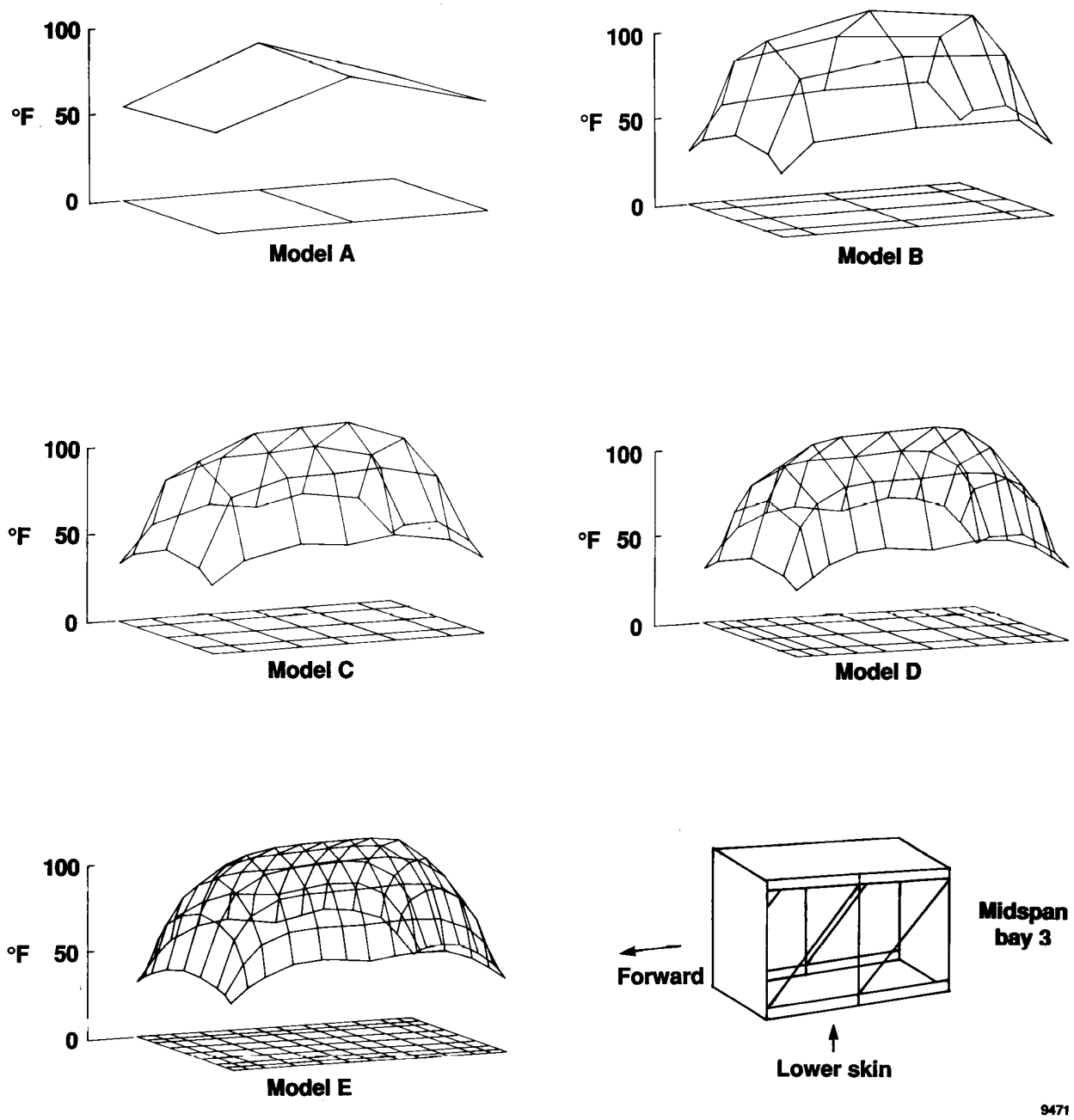

Figure 6. Distributions of orbiter wing lower skin temperatures predicted from thermal models A, B, C, D, E; time = 1,700 sec, STS-5.

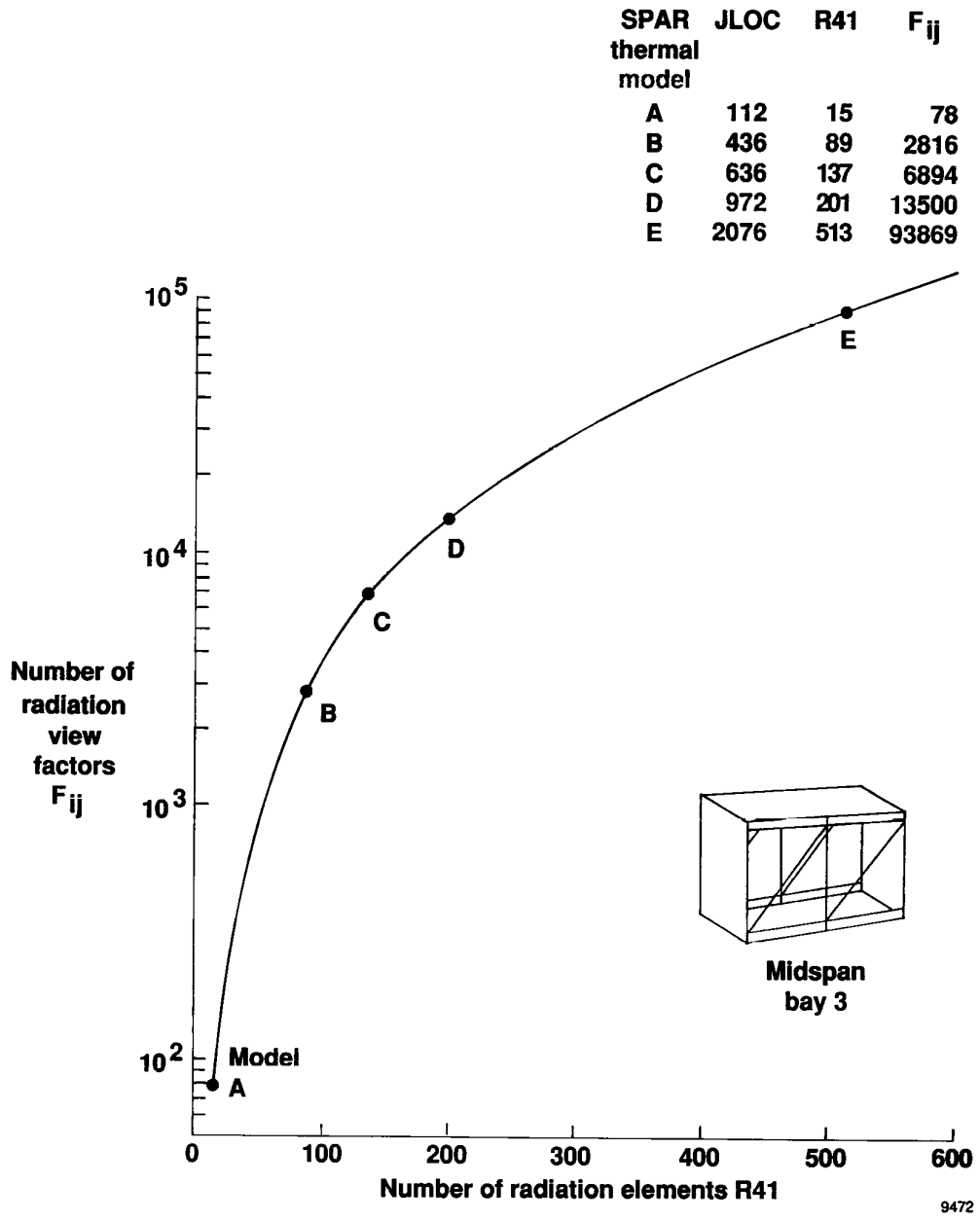

Figure 7. Number of radiation view factors as a function of number of radiation elements, orbiter wing midspan bay 3.

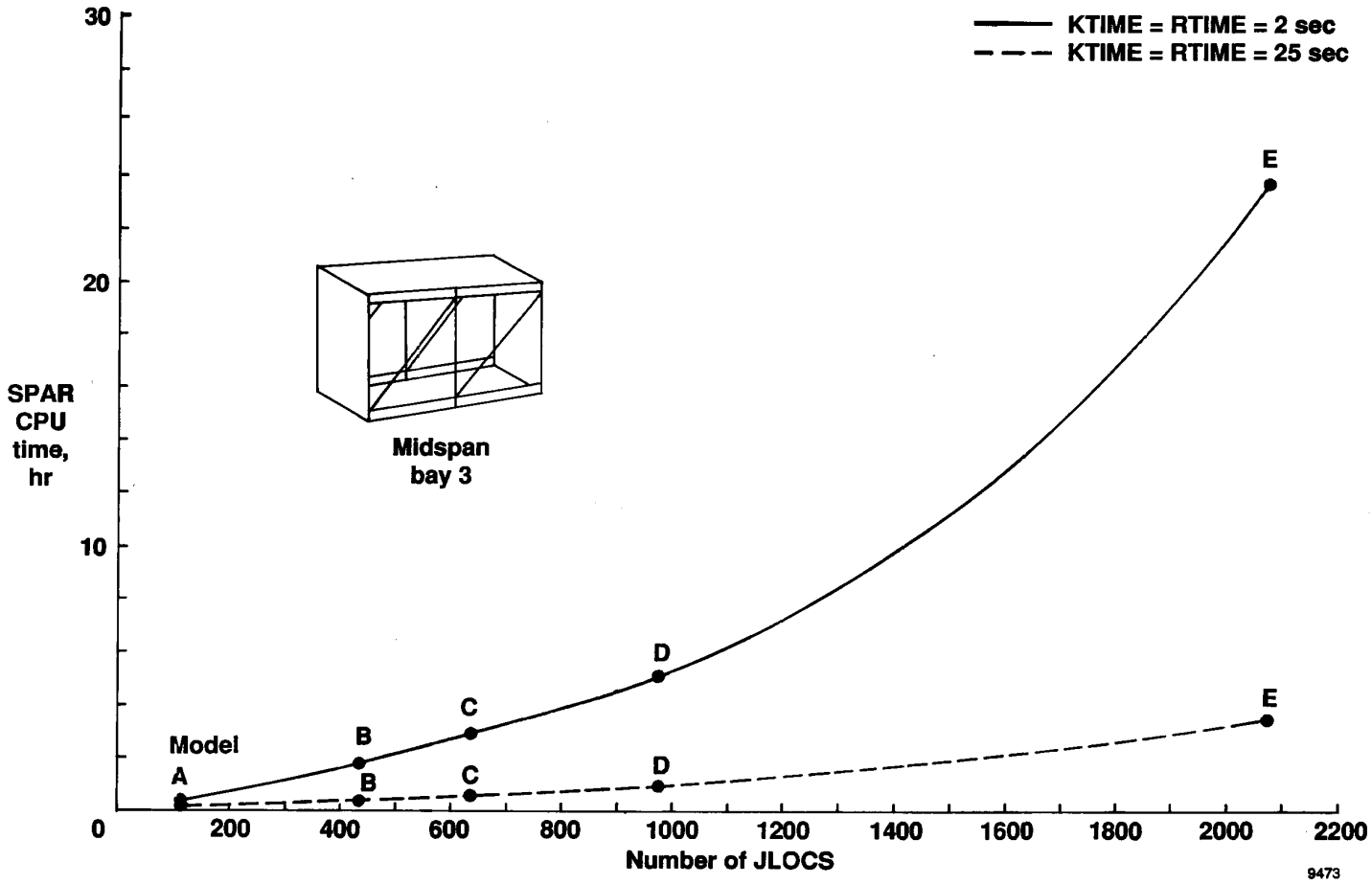

Figure 8. SPAR computation CPU time as a function of number of joint locations, $T_2 = 3000$ sec.

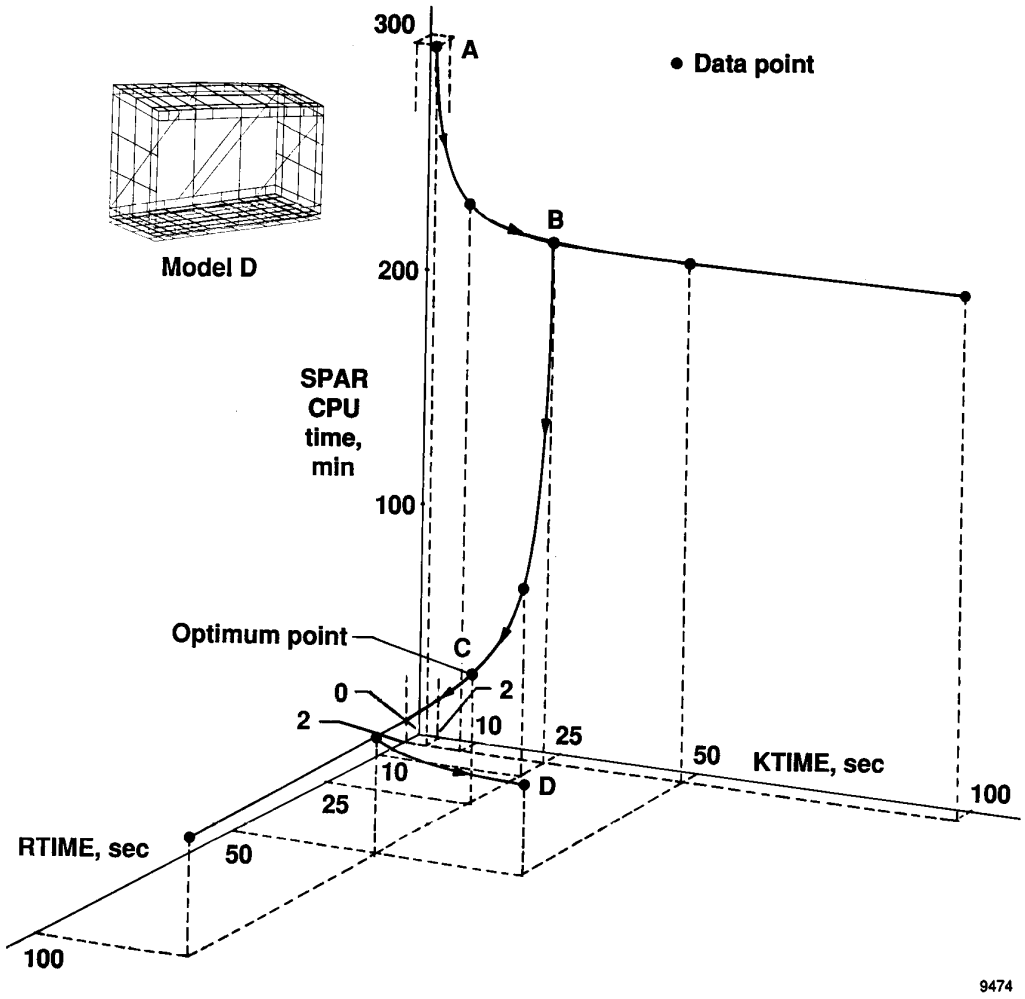

Figure 9. Three-dimensional plots of SPAR CPU time in KTIME–RTIME space.

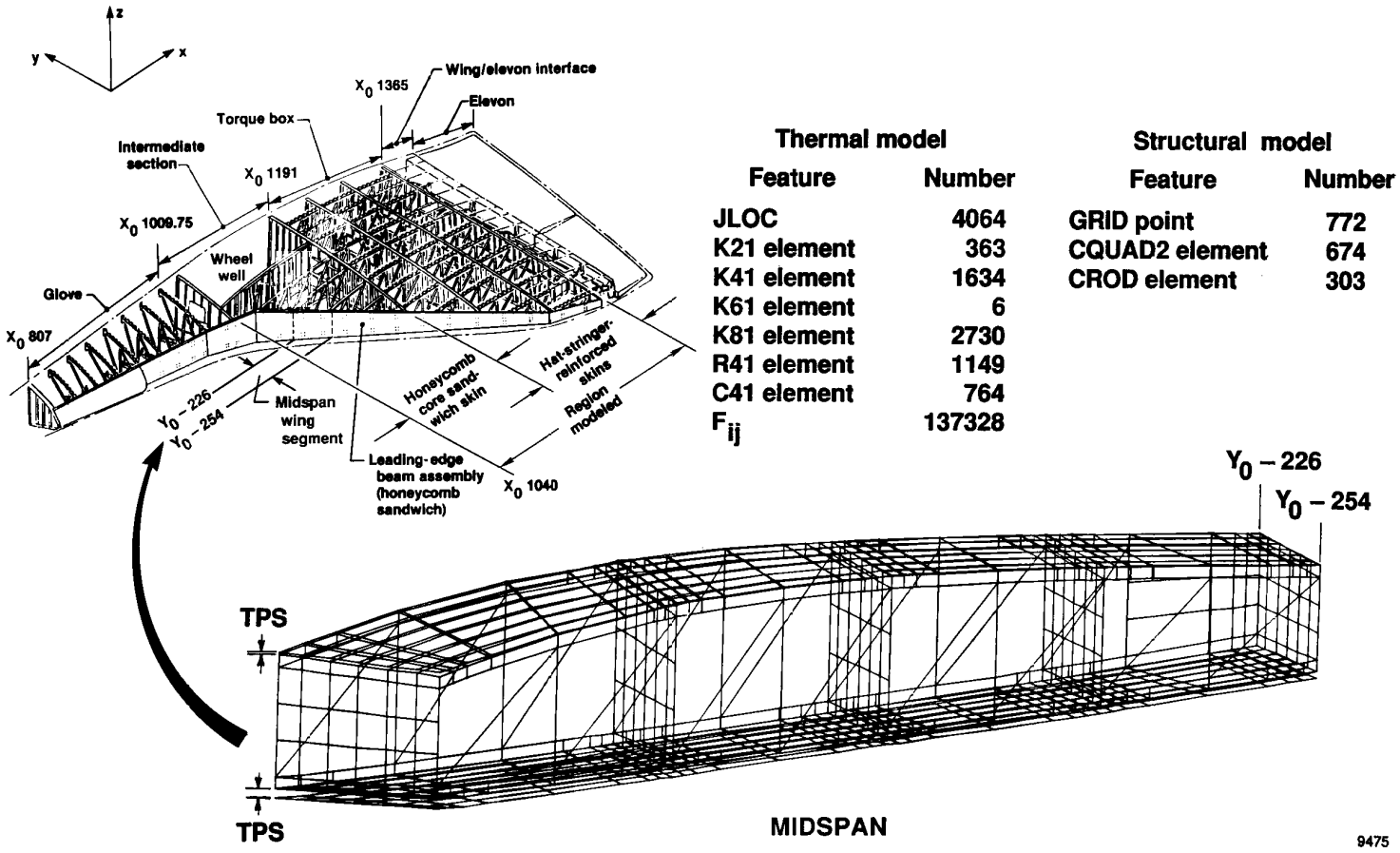

Figure 10. SPAR thermal model MIDSPAN setup for orbiter wing midspan segment; TPS removed to convert to structural model.

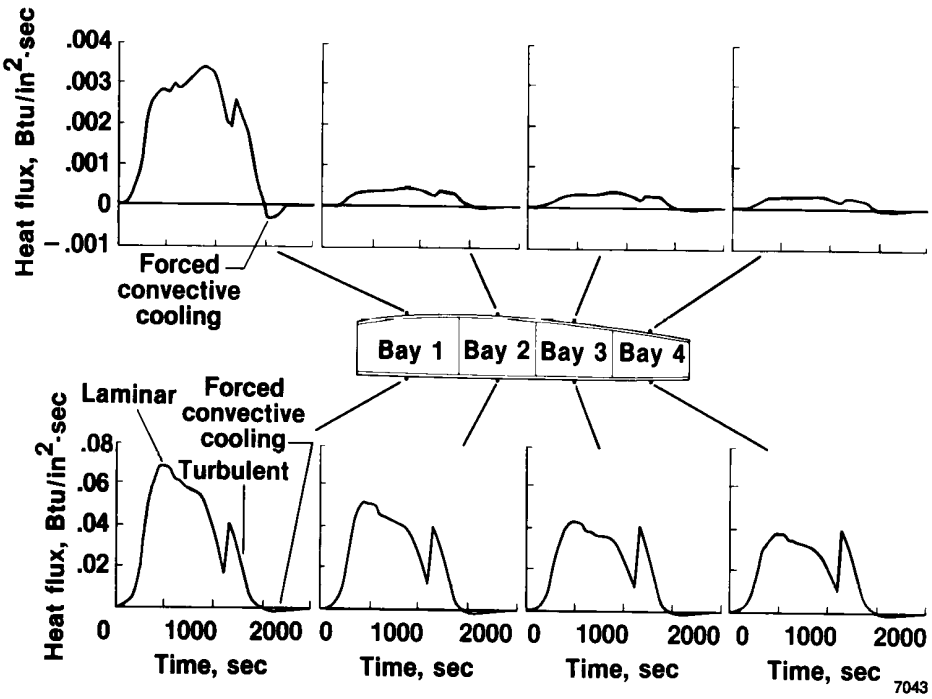

Figure 11. Surface heating rates at $|Y_o|240$; STS-5.

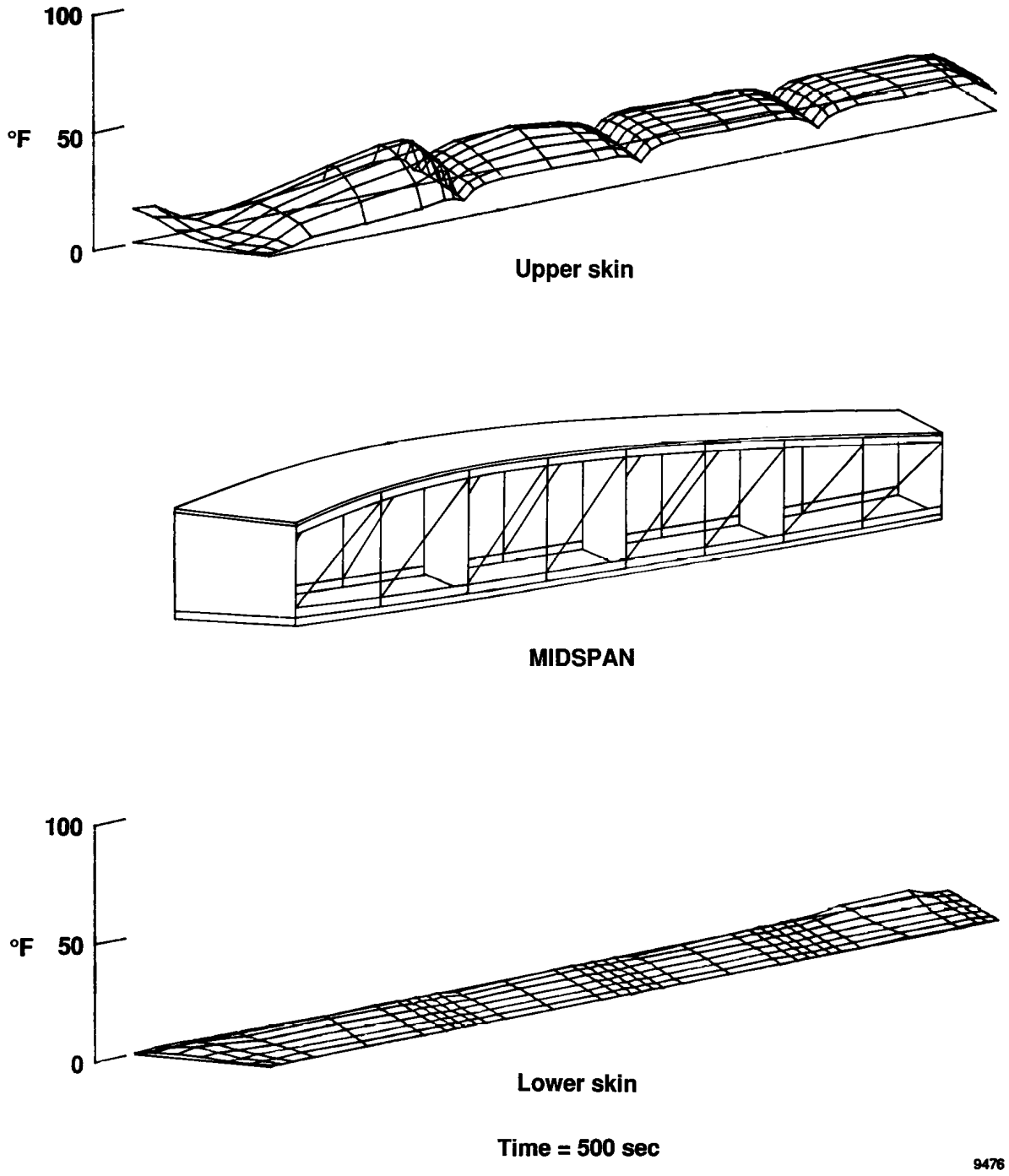

Figure 12. Orbiter wing skin temperature distributions.

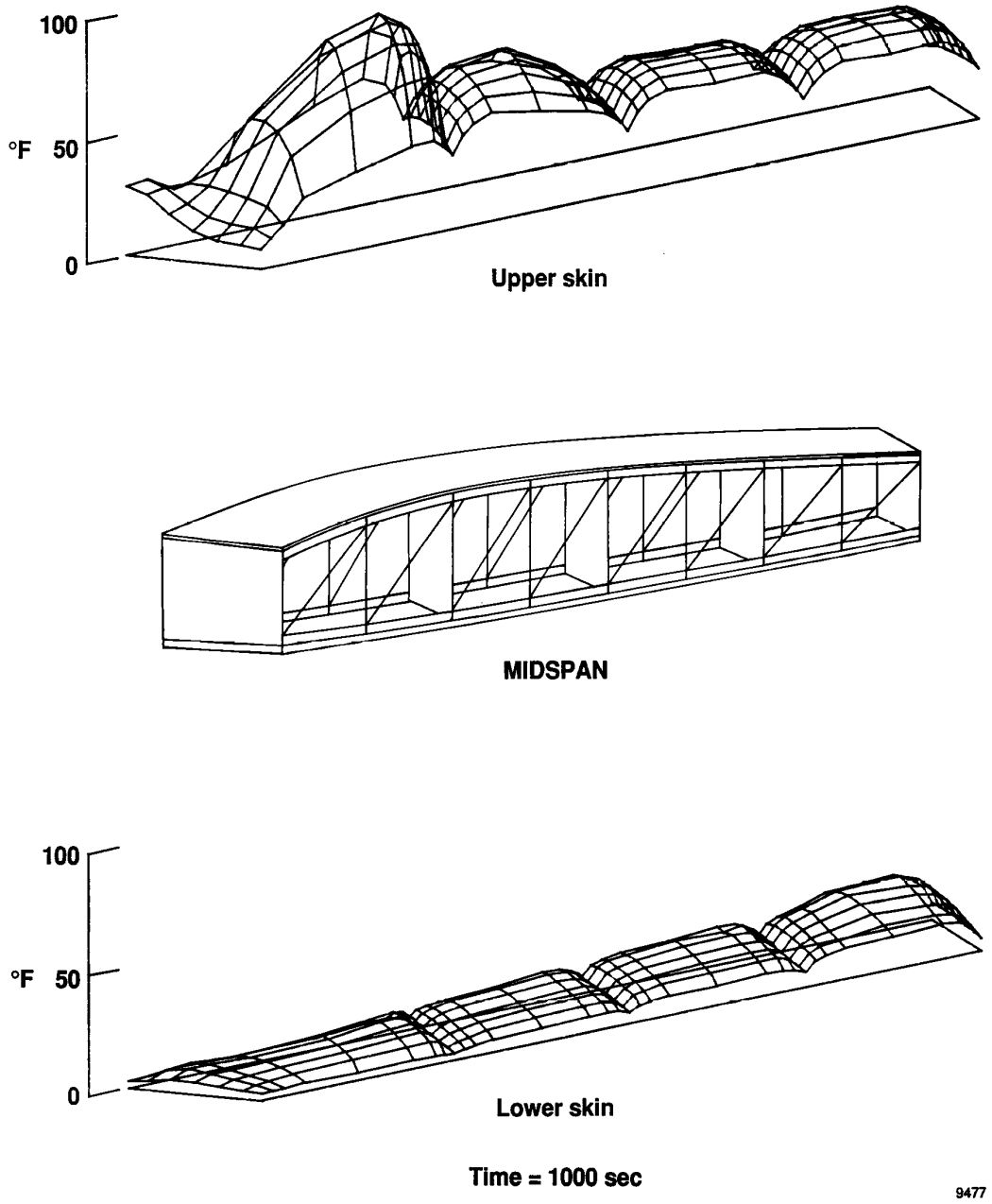

Figure 12. Continued.

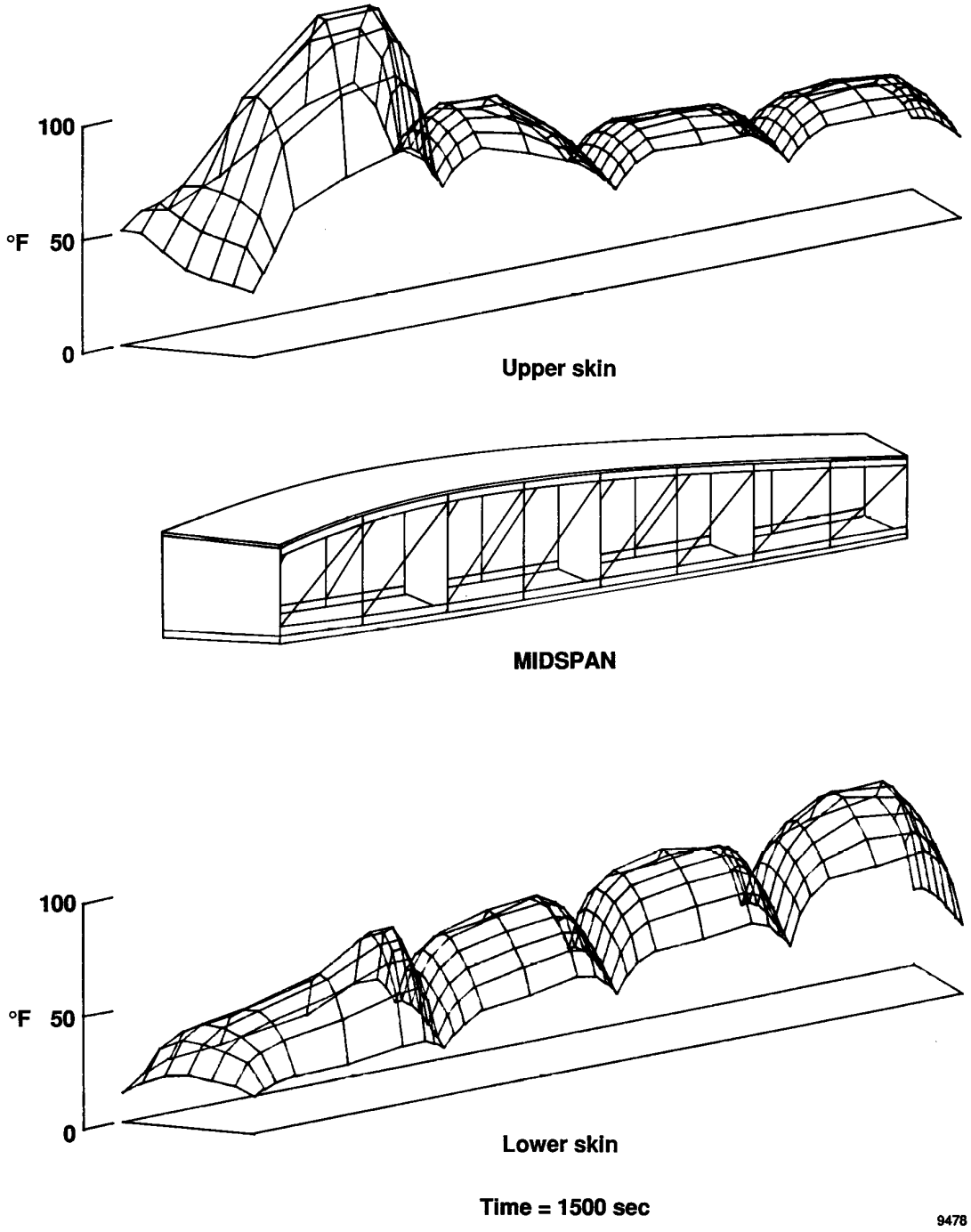

Figure 12. Continued.

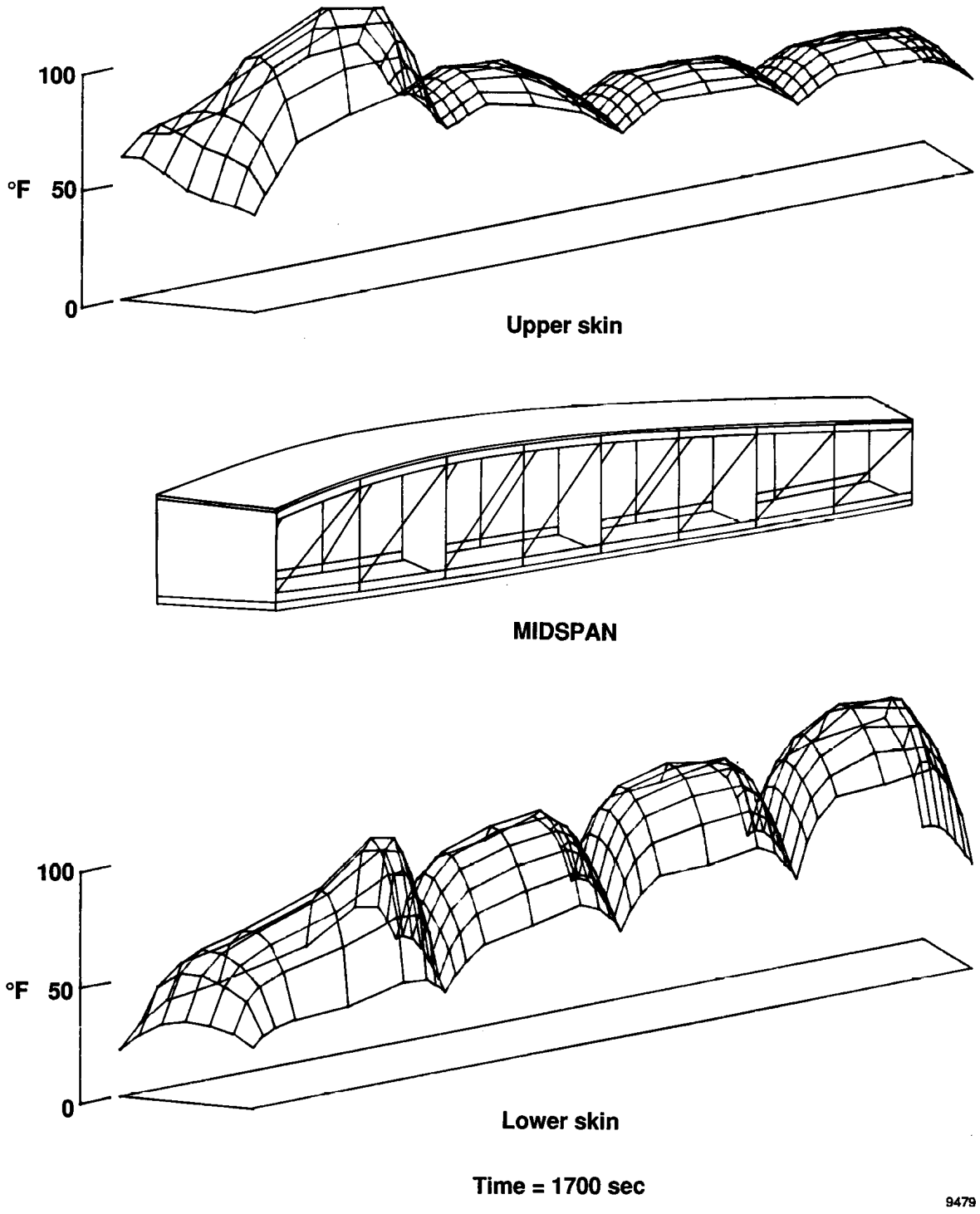

Figure 12. Continued.

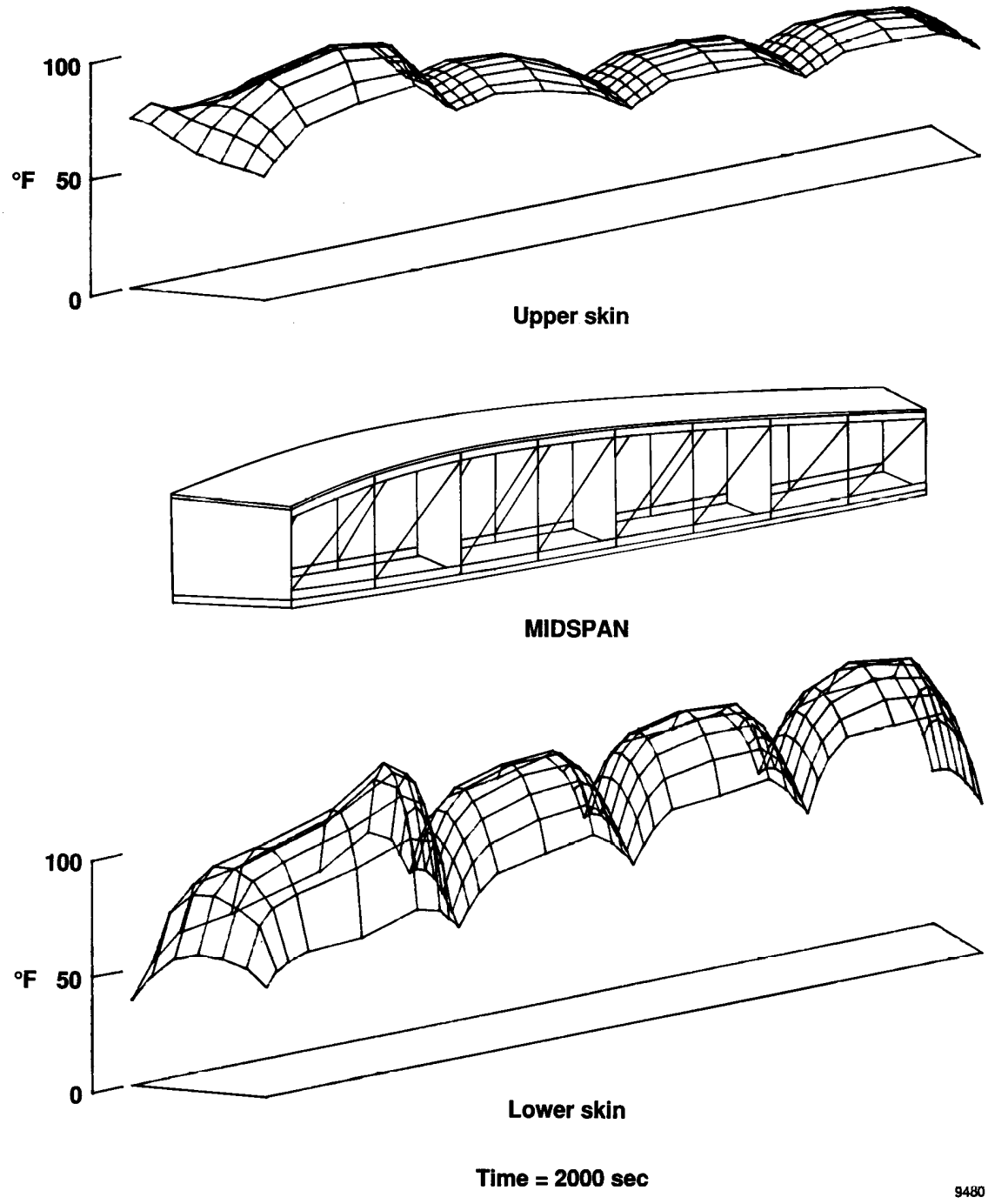

Figure 12. Continued.

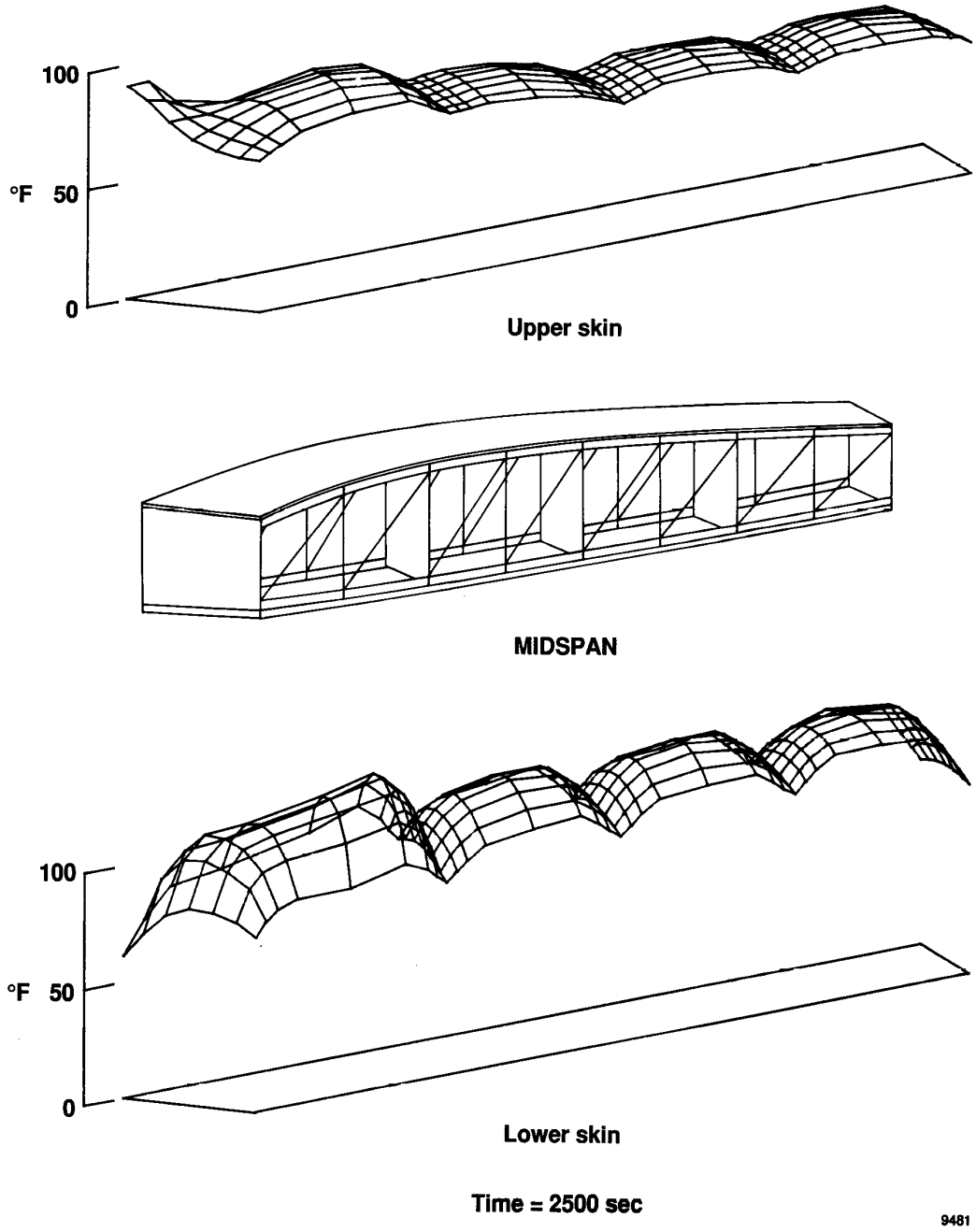

Figure 12. Continued.

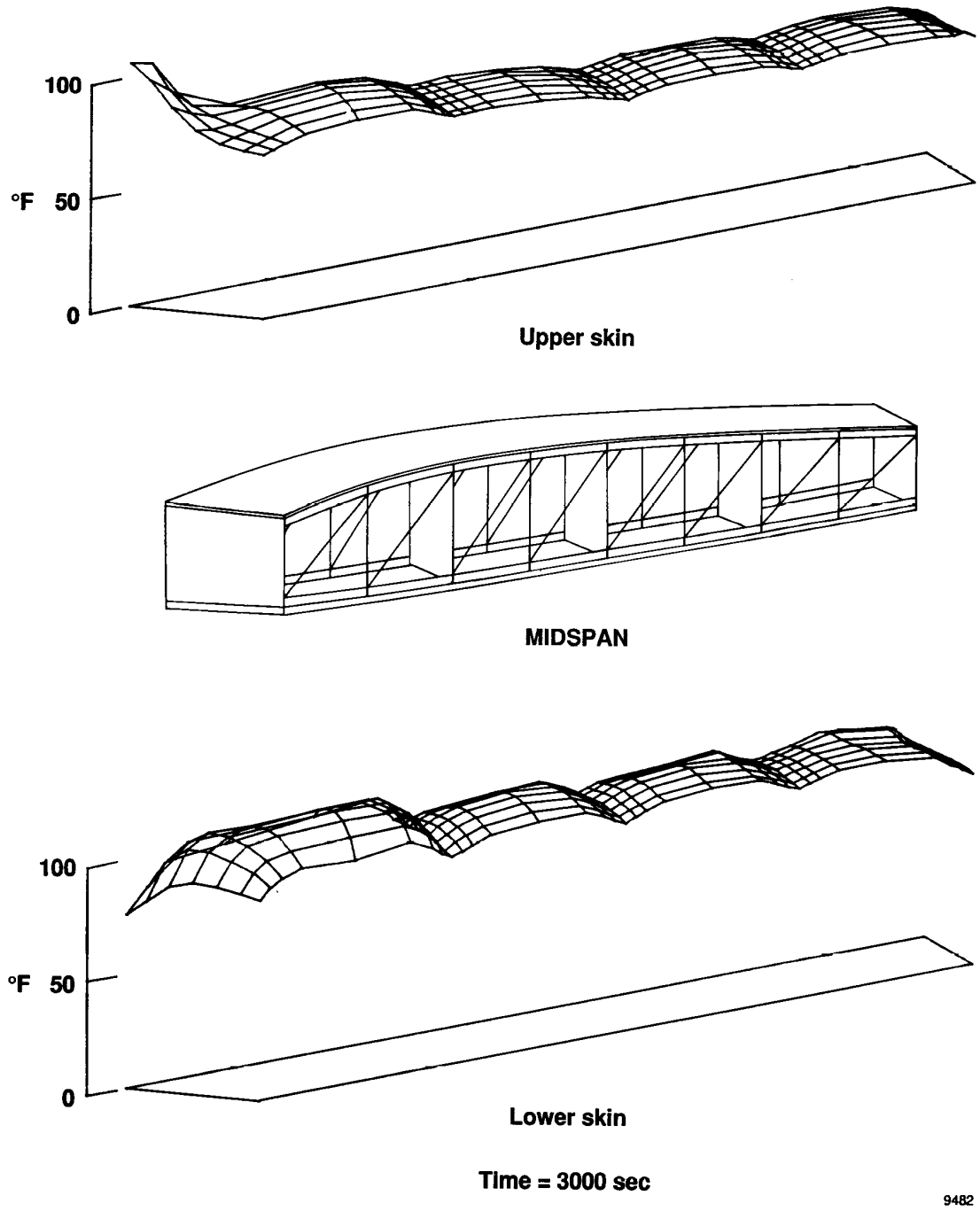

Figure 12. Concluded.

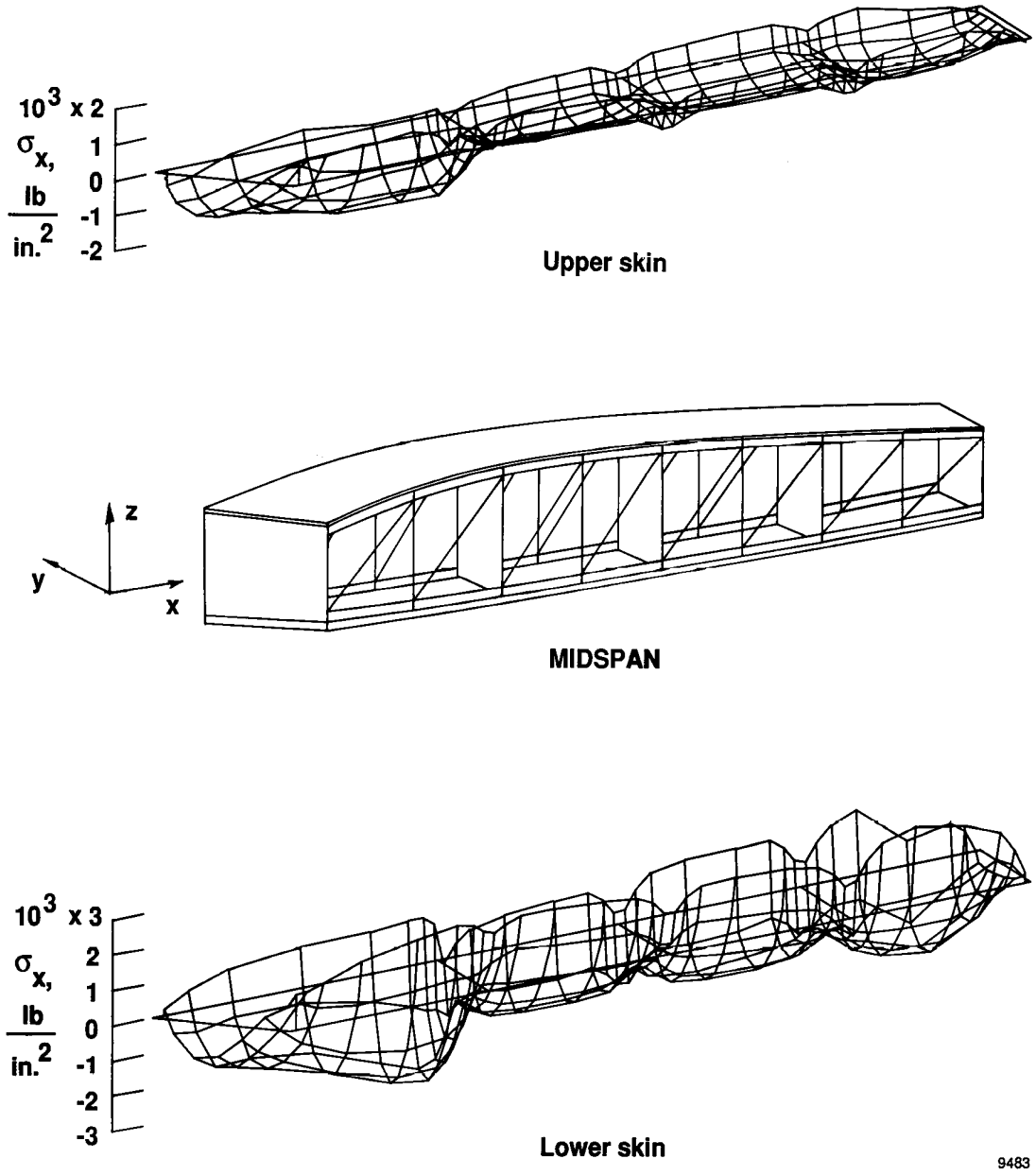

Figure 13. Distributions of chordwise stress σ_x in orbiter wing skins; time = 1700 sec, STS-5.

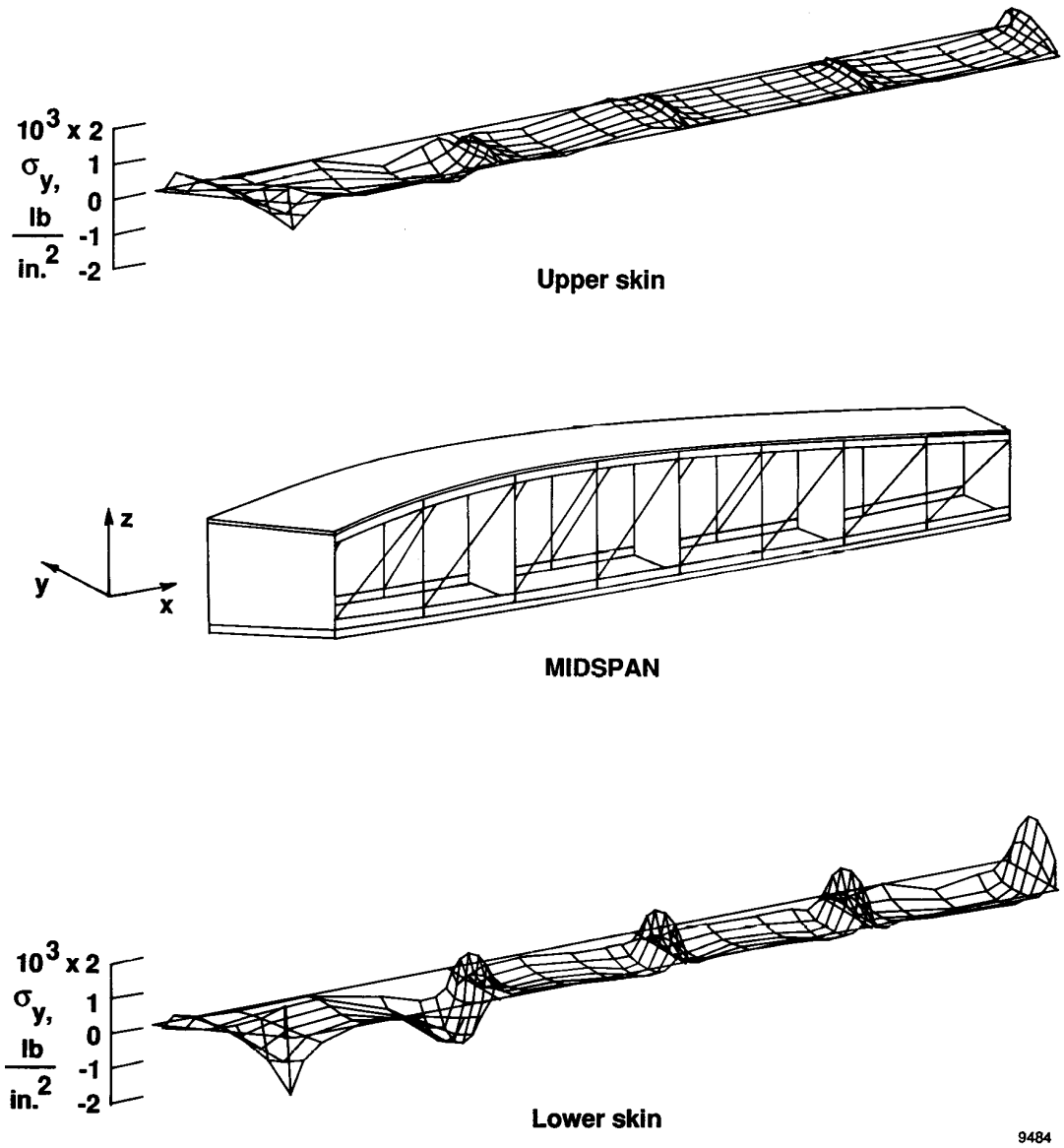

Figure 14. Distributions of spanwise stress σ_y in orbiter wing skins; time = 1700 sec, STS-5.

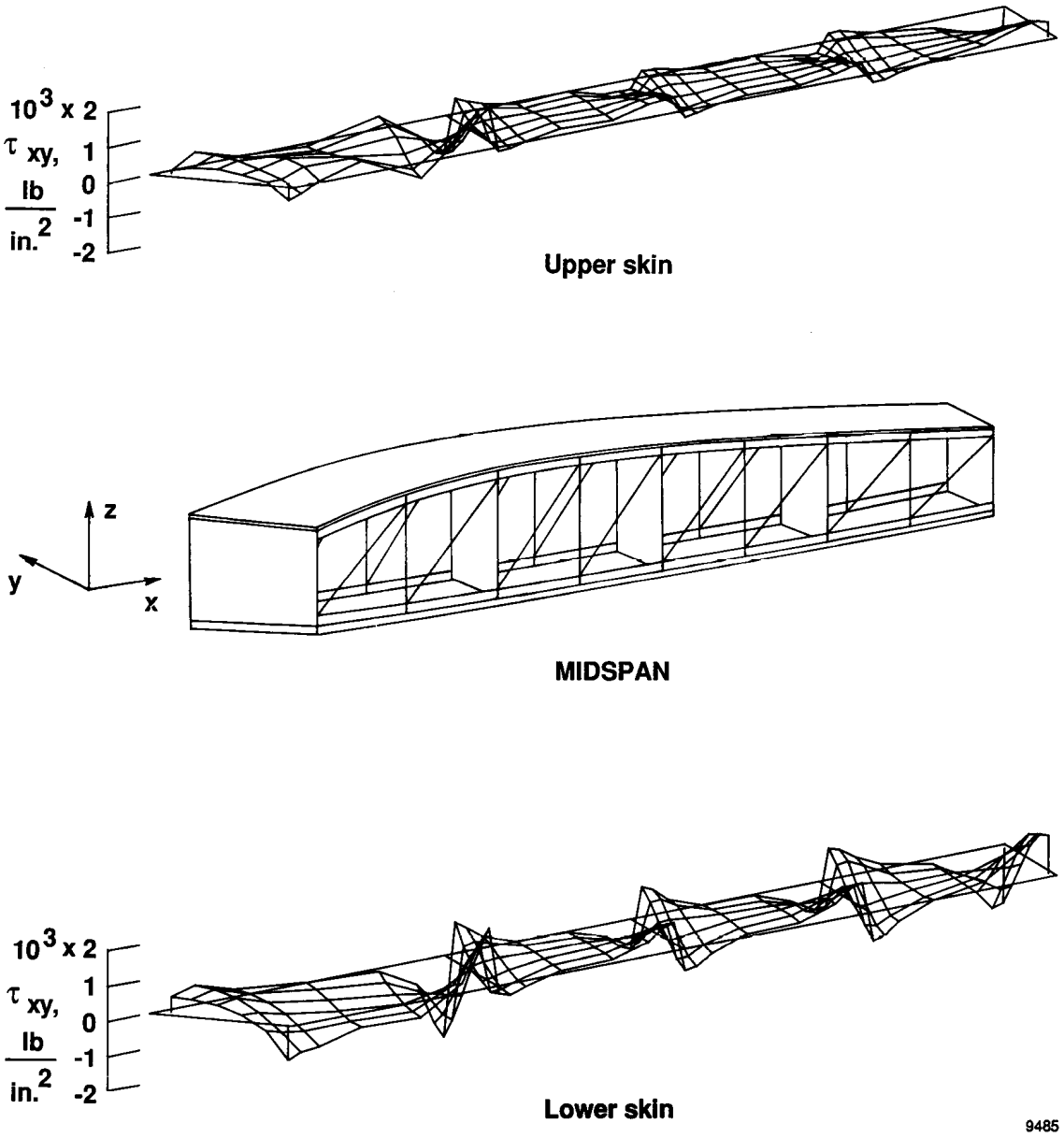

Figure 15. Distributions of shear stress τ_{xy} in orbiter wing skins; time = 1700 sec, STS-5.

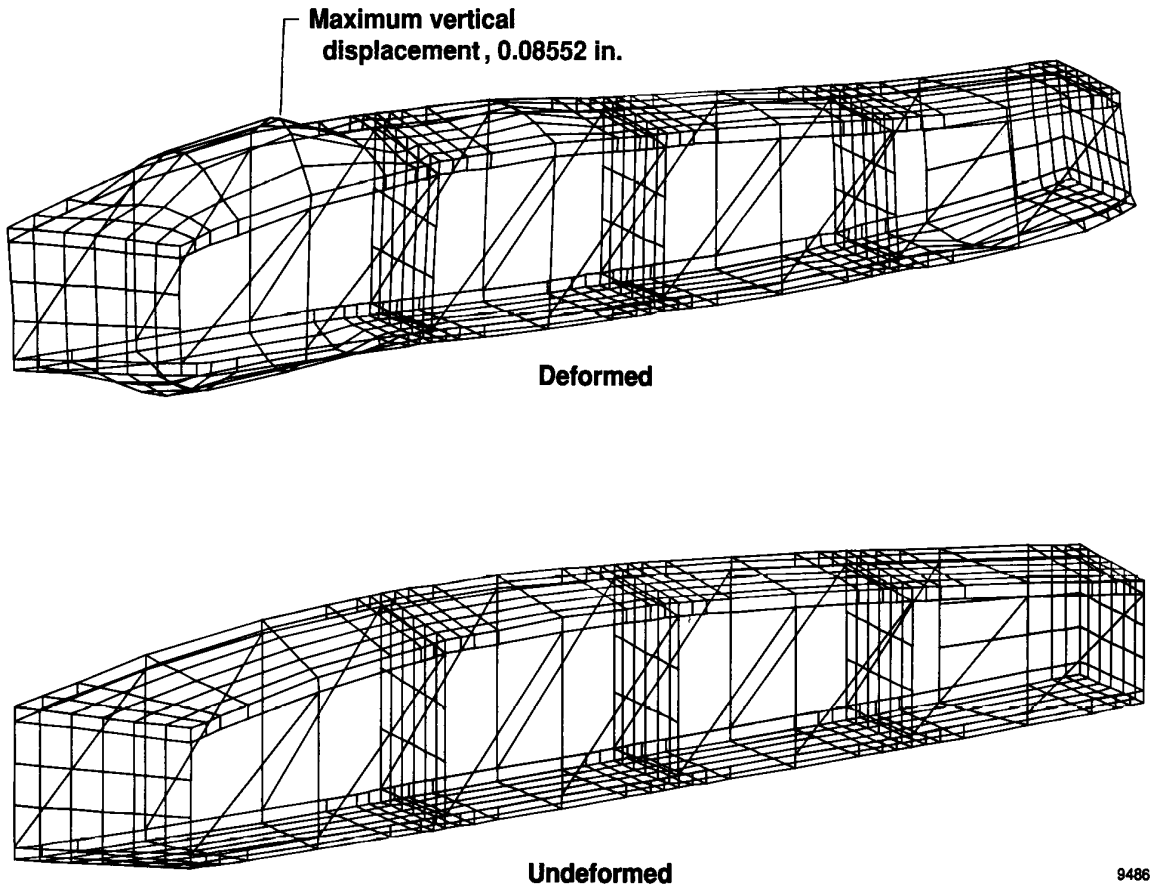

Figure 16. Deformed shape of orbiter wing midspan segment; time = 1700 sec, STS-5.

NASA
National Aeronautics and Space Administration

Report Documentation Page

1. Report No.	2. Government Accession No.	3. Recipient's Catalog No.
NASA TM-4163		

4. Title and Subtitle

Optimum Element Density Studies for Finite-Element Thermal Analysis of Hypersonic Aircraft Structures

5. Report Date

January 1990

6. Performing Organization Code

7. Author(s)

William L. Ko, Timothy Olona, and Kyle M. Muramoto

8. Performing Organization Report No.

H-1519

10. Work Unit No.

RTOP 532-09-01

9. Performing Organization Name and Address

NASA Ames Research Center
Dryden Flight Research Facility
P.O. Box 273, Edwards, CA 93523-5000

11. Contract or Grant No.

13. Type of Report and Period Covered

Technical Memorandum

12. Sponsoring Agency Name and Address

National Aeronautics and Space Administration
Washington, DC 20546

14. Sponsoring Agency Code

15. Supplementary Notes

16. Abstract

Different finite-element models previously set up for thermal analysis of the space shuttle orbiter structure were discussed and their shortcomings were identified. Element density criteria were established for the finite-element thermal modelings of space shuttle orbiter-type large, hypersonic aircraft structures. These criteria were based on rigorous studies on solution accuracies using different finite-element models having different element densities set up for one cell of the orbiter wing. Also, a method for optimization of the transient thermal analysis computer central processing unit (CPU) time was discussed. Based on the newly established element density criteria, the orbiter wing midspan segment was modeled for the examination of thermal analysis solution accuracies and the extent of computation CPU time requirements. The results showed that the distributions of the structural temperatures and the thermal stresses obtained from this wing segment model were satisfactory and the computation CPU time was at the acceptable level. The studies offered the hope that modeling the large, hypersonic aircraft structures using high-density elements for transient thermal analysis was possible if a CPU optimization technique was used.

17. Key Words (Suggested by Author(s))	18. Distribution Statement
Finite-element solution accuracies; Radiation view factors; Reentry heat transfer; Space shuttle orbiter; Thermal stresses	Unclassified — Unlimited Subject category 34

19. Security Classif. (of this report)	20. Security Classif. (of this page)	21. No. of pages	22. Price
Unclassified	Unclassified	40	A03

NASA FORM 1626 OCT 86

**For sale by the National Technical Information Service, Springfield, VA 22161-2171.*

NASA-Langley, 1990